Supporting Information for

Interfacial degradation of the NMC/Li_6PS_5Cl composite cathode in all-solid-state batteries

Xudong Hu,[a] Zishuo Zhao,[b] Yang Zhao,[a] Xuelong Wang,[c] Sami Sainio,[d] Dennis Nordlund,[d] Cristina M. Ruse,[e] Xiao-Dong Zhou,[e] Shannon W. Boettcher,[a] Dong Hou,*[e] Qi-Jun Hong,*[b] and Linqin Mu,*[b]

[a] Department of Chemistry and Biochemistry and the Oregon Center for Electrochemistry, University of Oregon, Eugene, OR 97403, USA

[b] School for Engineering of Matter, Transport, and Energy, Arizona State University, Tempe, 85287, USA

[c] Chemistry Division, Brookhaven National Laboratory, Upton, NY 11973, USA

[d] Stanford Synchrotron Radiation Lightsource, SLAC National Accelerator Laboratory, Menlo Park, CA 94025, USA

[e] Institute for Materials Research and Innovation (IMRI), University of Louisiana at Lafayette, Lafayette, LA 70503, USA

*Corresponding author.

E-mail address: linqinmu@asu.edu
qhong7@asu.edu
dong.hou@louisiana.edu

Supporting Tables

Table S1: The SOC values corresponding to each Nyquist plot, along with the fitting parameters R_{Ω}, $R_{ct,a}$, and $R_{ct,c}$ from the equivalent circuit depicted in Fig. S1, were listed during the initial charging process.

Charging time / h	SOC value / V vs. Li/Li^+	R_{Ω} /Ω	$R_{ct,a}$/Ω	$R_{ct,c}$/Ω
1	3.77	46.56	18.94	576.7
2	3.81	45.71	18.37	599
3	3.84	46.86	19.47	654
4	3.86	46.44	22.67	697.5
5	3.89	45.9	25.41	749.8
6	3.92	45.24	27.75	803.6
7	3.96	45.56	28.67	863.9
8	4.00	45.2	28.94	926.7
9	4.04	44	30.84	1002
10	4.09	45.15	30.72	1126
11	4.14	45.88	32	1311
12	4.20	45.36	34.13	1554
13	4.26	47.88	33.42	1889
14	4.33	48.22	34.09	2318
15	4.41	48.72	35.64	3005
16	4.49	47.91	36.19	3947
17	4.58	46.83	39.23	5417

Table S2: Fitted values of R_{Ω}, $R_{ct,a}$, and $R_{ct,c}$ of the equivalent circuit described in Fig. S1 used to model the impedance responses of the cell during the standing time after the cell was charged to 4.0 and 4.25 V.

	Standing time / h	R_{Ω} / Ω	$R_{ct,a}$ / Ω	$R_{ct,c}$/Ω
After the cell was charged to 4.0 V	0	38.71	114.5	1269
	1	38.64	119.6	1406
	2	37.65	123.6	1475
	3	38.21	126.5	1542
	4	37.81	129.1	1588
	5	37.11	131.4	1621
	6	37.49	131.8	1647
	7	36.38	136.2	1693
	8	37.98	135.7	1713
	9	37.99	135.8	1728
	10	36.86	136.2	1734
	11	37.84	135.1	1738
	12	37.44	135.1	1738
After the cell was charged to 4.25 V	0	36.94	125.9	2262
	1	37.01	125.8	2320
	2	38.99	125.2	2371
	3	37.41	128.3	2390
	4	37.22	129.3	2407
	5	36.84	135.5	2507
	6	37.89	140	2631
	7	37.34	148.5	2789
	8	37.87	154.3	2912
	9	37.97	158.6	2974
	10	35.22	164	3023
	11	35.84	163.9	3039
	12	36.56	163.7	3038

Table S3 Peak assignments for the pure Li_6PS_5Cl.

Raman shift / cm^{-1}	Assignment	Reference
199	PS_4^{3-}	[11]
272	Δ_{def}(S-P-S) in PS_4^{3-}	[12]
425	$\upsilon_s(PS_4^{3-})$ in PS_4^{3-}	[12]
573 600	PS_4^{3-}	[11]

Preparations for the ICP test and the ICP results

Preparation of the standard solutions:

Standard solutions were a series of LiCl solutions with different concentrations of Li. They were used to get a linear plot to measure the concentration of Li in unknown solutions (25%-deli NMC532, 50%-deli NMC532, and 75%-deli NMC532). The preparation details are as follows: 1000 ppm Li solution (Agilent Technologies) was used as the mother solution. Standard-1, -2, -3, -4, and -5 were made by diluting 1.91, 1.94, 1.97, 2.05, and 1.92 mother solution to 18.99, 24.25, 48.99, 99.85, and 187.68 g, respectively. The resulting Li concentrations in the standard solutions are shown in Table S4.

Table S4. Li concentrations in the standard solutions

Standard solutions	Li (ppm)
Standard-1	100.56
Standard-2	80.01
Standard-3	40.21
Standard-4	20.53
Standard-5	10.23

Preparation of the unknown solutions:

The unknown solution was prepared with the NMC532 or chemically delithiated NMC532 sample. Before weighing, the powders (25%-deli NMC532, 50%-deli NMC532, and 75%-deli NMC532) were vacuumed dried at 70 ℃ overnight. 30.01, 30.05, 30.02 mg of dried 25%-deli NMC532, 50%-deli NMC532, and 75%-deli NMC532, respectively, were added in 20 mL hydrochloric acid and nitric acid solution (0.2 M HCl and 0.4 M HNO_3). The suspensions stood for 12 h to ensure the delithiated NMC532 samples were completely dissolved. The solutions of 25%-deli NMC532, 50%-deli NMC532, and 75%-deli NMC532 were diluted to 100.0, 100.0, and 100.2 g, respectively, with deionized water to give the resultant unknown solutions with concentrations as shown in Table S5.

Table S5. Concentrations of the unknown solutions.

Unknown solution	Concentration (ppm)
25%-deli NMC532	1000.1
50%-deli NMC532	1011.5
75%-deli NMC532	1020.35

Table S6. ICP results for 25%-deli NMC532, 50%-deli NMC532, and 75%-deli NMC532

Sample	Measured Concentration of Li / ppm	Calculated x value in $Li_xNi_{0.5}Mn_{0.3}Co_{0.2}O_2$
25%-deli NMC532	61.59	0.84
50%-deli NMC532	51.73	0.69
75%-deli NMC532	41.3	0.54

Supporting Figures

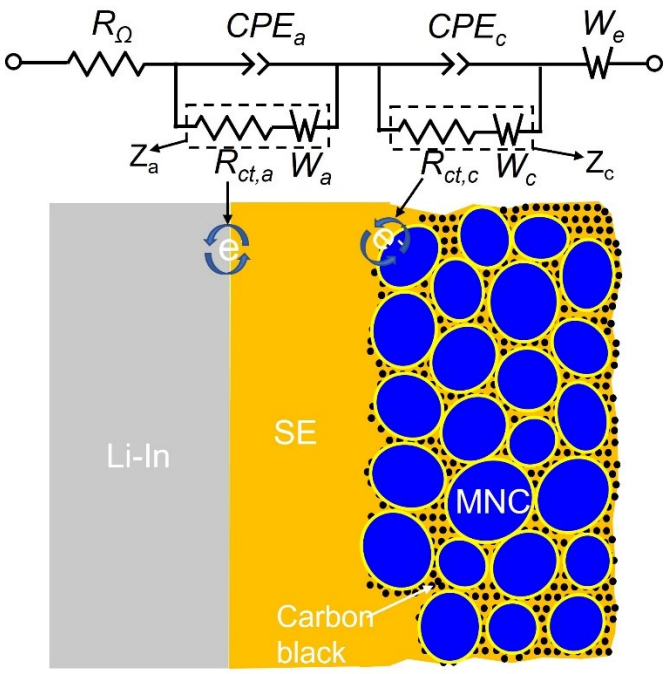

Fig. S1 Equivalent circuit that was used for the fitting of the impedance spectra, the bottom Fig. is the schematic configuration of the ASSB. R_Ω represents the ohmic resistance of the cell (resistance mainly from solid-state electrolyte since carbon additives were used in the composite cathode), corresponding to impedance contributions in the high-frequency region. The parallel combination of $CPE_{a/c}$ and $Z_{a/c}$ represents the impedance contributions that correspond the interface reactions (double-layer and Faradic processes) between the solid electrolyte and anode/cathode active material, corresponding to impedance contributions in the medium-frequency region. The CPE (constant phase element) models the behavior of double layer process which can be considered as an imperfect capacitor. Z models the Faradic process and is a serial combination of the charge-transfer resistance (R_{ct}) and the mass-transfer impedance (or Warburg impedance). W_e, W_a, and W_c represent the Warburg impedances due to the mass transfer in the solid electrolyte, anodic side, and cathodic side, respectively.

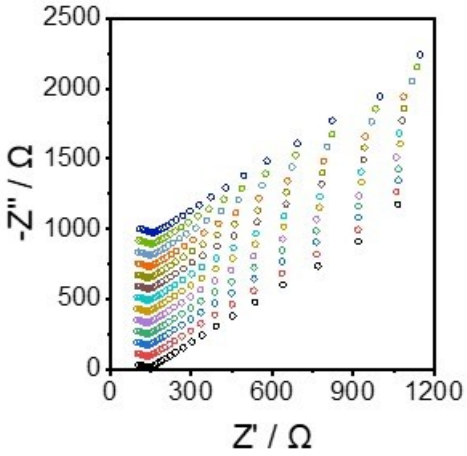

Fig. S2 Nyquist plots of the ASSB (time increases from the bottom up) that were collected in Zone 1.

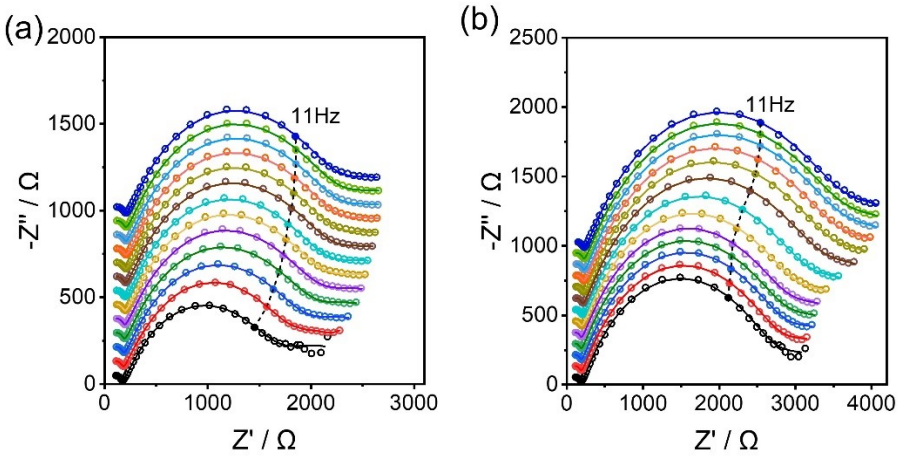

Fig. S3 Nyquist plots of the ASSB that were collected in (a) Zone 3 and (b) Zone 4, and corresponding fitted data based on the equivalent circuit described in Fig. S1 (circles for raw data and solid lines for fitted data).

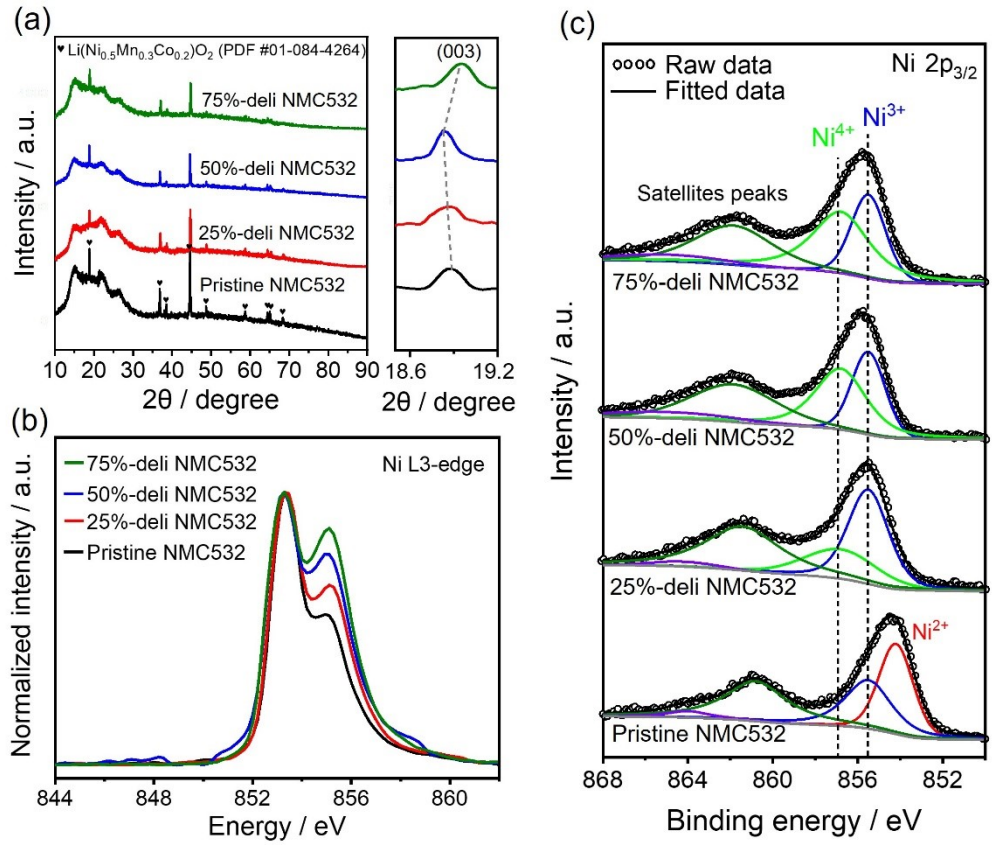

Fig. S4 X-ray characterizations of pristine and chemically-delithiated NMC532 cathode materials. (a) XRD patterns of the samples, the samples were sealed with Kapton tape to avoid exposure in air during the measurement. All the peaks in the XRD patterns can be indexed to a rhombohedral $LiNi_{0.5}Mn_{0.3}Co_{0.2}O_2$ structure (PDF # 01-084-4264).[1] The shift of (003) peak of the samples has the same trend as the reported in situ XRD results,[2,3] demonstrating the success of the chemical delithiation of NMC532. (b) soft XAS (X-ray absorption spectroscopy) spectra of Ni L_3-edge in the FY (fluorescence yield) mode. Nickel oxidation is primarily responsible for the charging capacity in NMC532 materials,[4,5,] and can be used as a benchmark to evaluate the global delithiation of NMC532. The FY mode of soft XAS can measure the electronic properties of the subsurface (up to 100 nm) of particles, which can represent the bulk behavior. The splitting of the Ni L_3-edge is a result of the Ni2p-Ni3d electrostatic interaction and crystal field effects.[6] The increased intensity at Ni L3-right (~855 eV) indicates the increase of the Ni oxidation state with the increased degree of delithiation.[6,7] (c) XPS (X-ray photoelectron spectroscopy) spectra of Ni $2p_{3/2}$ to represent the surface oxidation state (~2 nm). The fitting results show that Ni oxidation states are $Ni^{2+/3+}$ and $Ni^{3+/4+}$ for the pristine NMC532 and chemically delithiated NMC532, respectively.[8-10] Note that the intensity ratio of Ni^{3+}/Ni^{4+} is close to each other between the 50%-delithiated NMC532 and 75%-delithiated NMC532 samples since the XPS is about the surficial measurement.

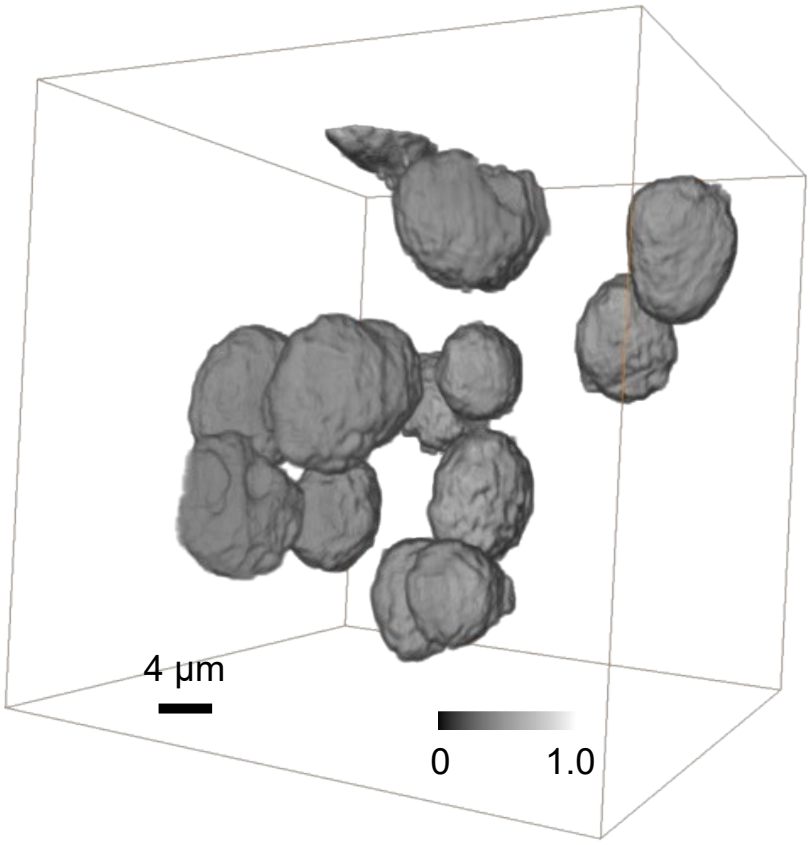

Fig. S5 Representative 3D rendering of synchrotron X-ray nano-tomography on NMC secondary particles. The box frame is the view field of tomography measurement, and each measurement captures tens of particles for reproducibility validation. The grey-scale rending uses a normalized Ni K-edge absorption coefficient.

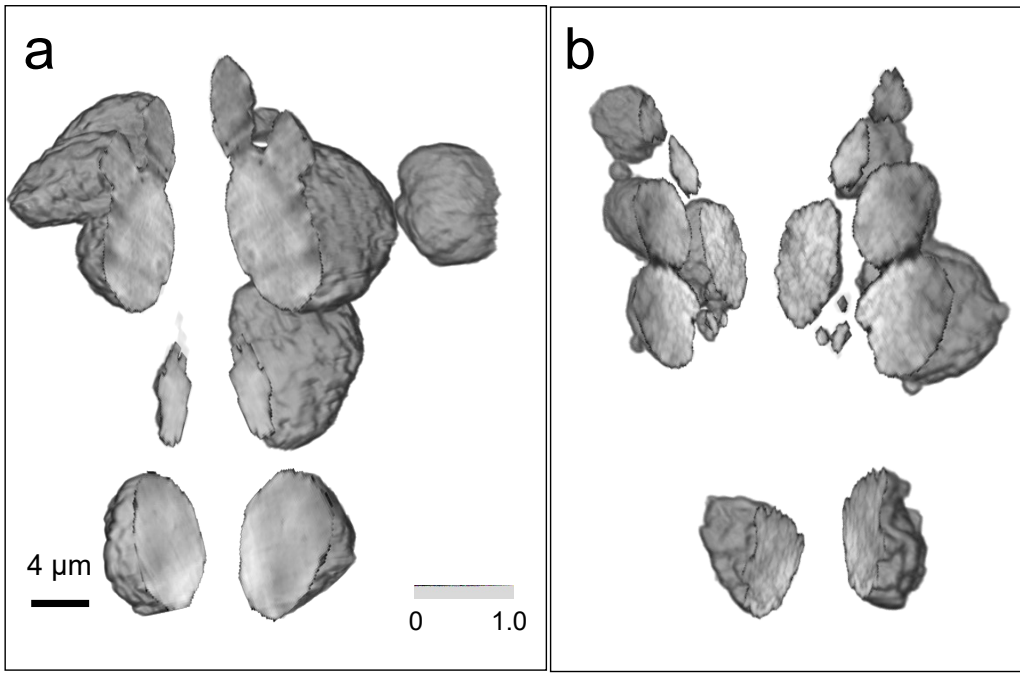

Fig. S6 Selected 3D rendering of particles with the cross-section images showing the interior morphology. (a) pristine NMCs and (b) 50%-delithiated NMCs. The grain boundaries in pristine NMCs are invisible due to the limitation of spatial resolution, while the cracks are obvious in 50%-delithiated NMCs, indicating the success of chemical delithiation.

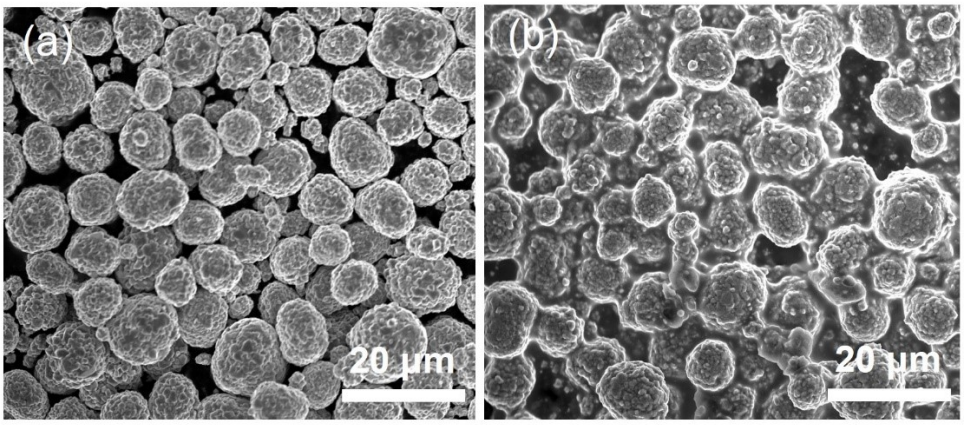

Fig. S7 SEM images of (a) 50%-delithiated NMC and (b) the mixture of 50%-delithiated NMC and LPSC in a mass ratio of 9 : 1.

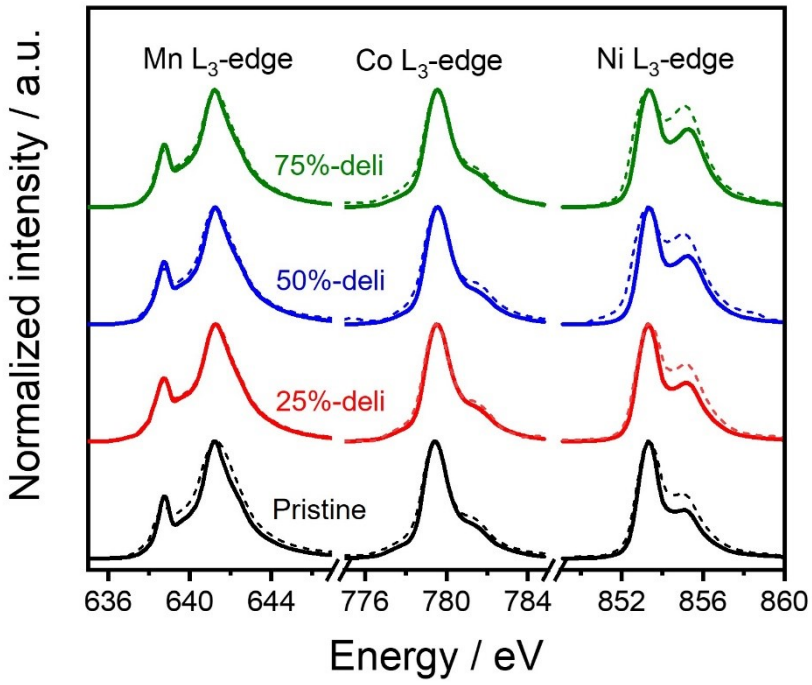

Fig. S8 Soft XAS spectra in TEY (solid line) and FY (dash line) modes for the pristine NMC, 25%-delithiated NMC, 50%-delithiated NMC532, and 75%-delithiated NMC532.

References

1 J. Kanthachan, O. Khamman, U. Intatha and S. Eitssayeam, *Mater. Today: Proceedings*, 2021, **47**, 3600-3603.

2 S.-W. Lee, D.-H. Jang, J.-B. Yoon, Y.-H. Cho, Y.-S. Lee, D.-H. Kim, W.-S. Kim and W.-S. Yoon, *J. Electrochem. Sci. Technol.*, 2012, **3**, 29-34.

3 J. Li, L. E. Downie, L. Ma, W. Qiu and J. R. Dahn, *J. Electrochem. Soc*., 2015, **162**, A1401-A1408.

4 Y. Yu, P. Karayaylali, L. Giordano, J. Corchado-Garcia, J. Hwang, D. Sokaras, F. Maglia, R. Jung, F. S. Gittleson and Y. Shao-Horn, *ACS Appl. Mater. Interfaces*, 2020, **12**, 55865-55875.

5 Y. Mao, X. Wang, S. Xia, K. Zhang, C. Wei, S. Bak, Z. Shadike, X. Liu, Y. Yang, R. Xu, P. Pianetta, S. Ermon, E. Stavitski, K. Zhao, Z. Xu, F. Lin, X. Q. Yang, E. Hu and Y. Liu, *Adv. Funct. Mater.*, 2019, **29**, 1900247.

6 F. Lin, D. Nordlund, I. M. Markus, T.-C. Weng, H. L. Xin and M. M. Doeff, *Energy. Environ. Sci.*, 2014, **7**, 3077.

7 L. Mu, J. Zhang, Y. Xu, C. Wei, M. M. Rahman, D. Nordlund, Y. Liu and F. Lin, *Nano Lett.*, 2022, **22**, 1278-1286.

8 Y. M. Wang, Y. J. Wang and F. Wang, *Nanoscale Res. Lett.*, 2014, **9**.

9 M. Zubair, G. Li, B. Wang, L. Wang and H. Yu, *ACS Appl. Energy Mater.*, 2018, **2**, 503-512.

10 M. Cheng, H. Fan, Y. Song, Y. Cui and R. Wang, *Dalton Trans.*, 2017, **46**, 9201-9209.